Modeling and Control Design for a Magnetic Levitation System

Manfredi Maggiore and Rafael Becerril*

Department of Electrical and Computer Engineering

University of Toronto, Toronto ON, Canada, M5S 3G4

maggiore@control.utoronto.ca becerril@ece.concordia.ca

Abstract

We study the problem of controlling the position of a platen levitated using linear motors in three-dimensional space. We develop a nonlinear six-state model of the system and provide two nonlinear controllers solving the set point stabilization problem. The first controller is derived by decomposing the model in two subsystems, applying feedback linearization to one of them, and using the invariance principle to prove attractiveness of the origin of the second subsystem. The second controller is found by dynamic feedback linearizing the entire system dynamics. In both cases we provide a rigorous procedure to determine the operating range of the device.

1 Introduction

Recent trends in the semiconductor industry show an increasing need to refine the photo-lithography process and achieve smaller line-widths ($< 0.13\mu$m). Currently in industry the photo-lithography stage is comprised of a lower-stage that actuates large high-speed movements and a flexure-based upper-stage that delivers high-precision movements in multiple degrees of freedom (Tsai and Yen 1999). The mechanical contacts can introduce impurities that may limit the accuracy of the photo-lithography process, thus decreasing production throughput. Further, the upper-stage flexure mechanism is driven by piezoelectric actuators that are capable of fine resolution but possess severe hysteresis nonlinearity (Tsai and Yen 1999). Mechanical contact problems and the inherent nonlinearities of piezoelectric actuators can be avoided by using planar magnetic levitation technology to move the platen.

Perhaps among the most successful research in this direction is the one reported in (Kim and Trumper 1998), where the authors use a linear controller to actuate a 6 DOF magnetic levitation device that achieves an x, y, z range of $50\text{mm}\times 50\text{mm}\times 400\mu$m using single sided air cored permanent magnet linear synchronous

*This work was supported by the Natural Sciences and Engineering Research Council of Canada (NSERC).

Published in *International Journal of Control* vol.77, 2004, no. 10, pp. 964–977

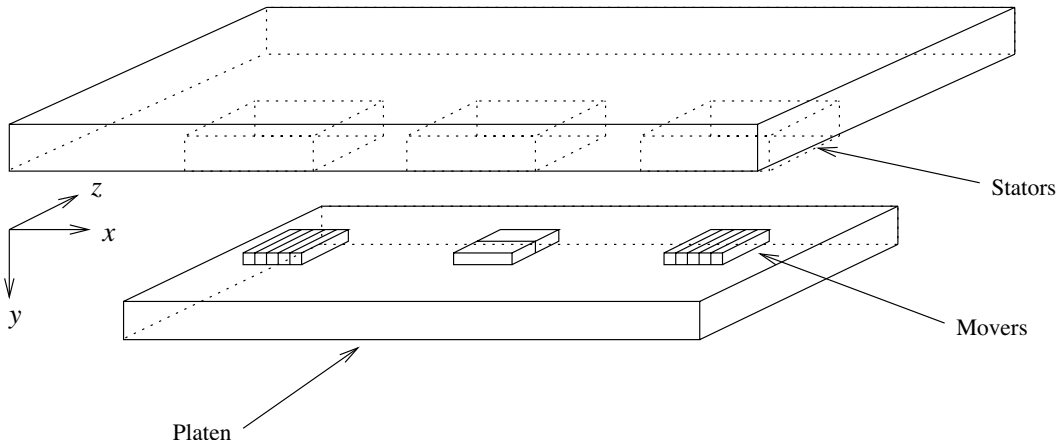

Figure 1: Configuration of three PMLSMs for three controlled degrees of freedom

motors (PMLSMs). Linear motors are indeed particularly suitable for magnetic levitation applications due to their superior range of operation.

Electromagnets can also be used for magnetic levitation, they are cheaper to build, easier to control than linear motors, but typically suffer from a smaller range of operation. This is seen, e.g., in (Shan, Kuo, Zhang and Menq 2002), where the authors use ten electromagnets to position a platen with six DOF over a range of $\pm 4 \times \pm 4$ mm^2 on the horizontal plane.

In this paper we study the theoretical properties of the *idealized* device shown in Figure 1, which employs three flat single sided *iron* cored PMLSMs to position a platen with three DOF. Our focus is in developing rigorous nonlinear control strategies to stabilize the platen at a desired (x, y, z) set point and in characterizing its range of operation. We stress that this is a theoretical study and the implementation of the design presented here will be the subject of future research. The modeling part of the paper relies on the work of Nasar and Xiong in (Nasar and Xiong 1988, Nasar and Xiong 1989), where a model of iron cored PMLSMs is developed. The model developed in (Nasar and Xiong 1988, Nasar and Xiong 1989) does not take into account the effect of the stator slots but lends itself to its consideration because it relies on the computation of the air-gap flux density, which is directly affected by the presence of slots. In the light of this observation, we adapt the work in (Zhu and Howe 1993) on the slot effect in permanent magnet DC rotary motors, and use it to model such effect in PMLSMs.

Major emphasis is placed on the control design problem. We prove stability of two nonlinear controllers. The first controller is derived by decomposing the model in two subsystems, applying feedback linearization to one of them, and using the invariance principle to prove attractiveness of the origin of the second subsystem. A procedure to estimate the domain of attraction of the equilibrium of the closed-loop system is provided. A drawback of this design is that the domain of attraction depends on the location of the

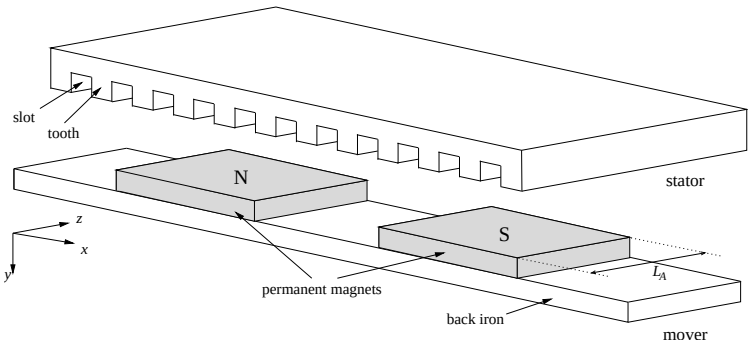

Figure 2: Structure of a permanent magnet linear synchronous motor

set point. To overcome this problem, we introduce a dynamic feedback linearizing controller and give necessary and sufficient conditions for it to make a *fixed* ellipsoidal set positively invariant for all set points in an predetermined interval.

2 The model of a PMLSM

In this section we derive a model for a flat single sided iron cored PMLSM made of a short *field* (or mover) moving underneath a stationary *armature* (or stator), as shown in Figure 2. In this device, permanent magnets occupy the surface of a flat structure of ferromagnetic material –the mover back iron. The stator is longitudinally laminated and transversally slotted in order to house a three-phase winding. Figure 3 shows the inertial coordinate frame used in the modeling procedure. As mentioned in the introduction, for this part we rely on the results of (Nasar and Xiong 1989) and (Zhu and Howe 1993). For the sake of illustration, we present a brief summary of the derivation of the expressions for the normal and longitudinal forces in a PMLSM, with emphasis on the differences between our analysis and that in (Nasar and Xiong 1989) and (Zhu and Howe 1993).

2.1 Magnetic field produced by the permanent magnets

In (Nasar and Xiong 1989), the authors calculate the magnetic potential produced by the permanent magnets, Ψ_{pm}, through the method of images and the concept of magnetic charge. Using the magnetic charge equivalence, they first describe the magnetic potential around the magnets by means of a system of partial differential equations. The method of images then solves such system of equations for Ψ_{pm} leading to an expression of the corresponding magnetic field intensity H_{pm}. Finally, the modeling uses H_{pm} to calculate the density of the magnetic flux B_{pm} around the permanent magnets.

Referring to Figures 2 and 3, let L_A be the *depth of each permanent magnet* along the z axis, h_m be

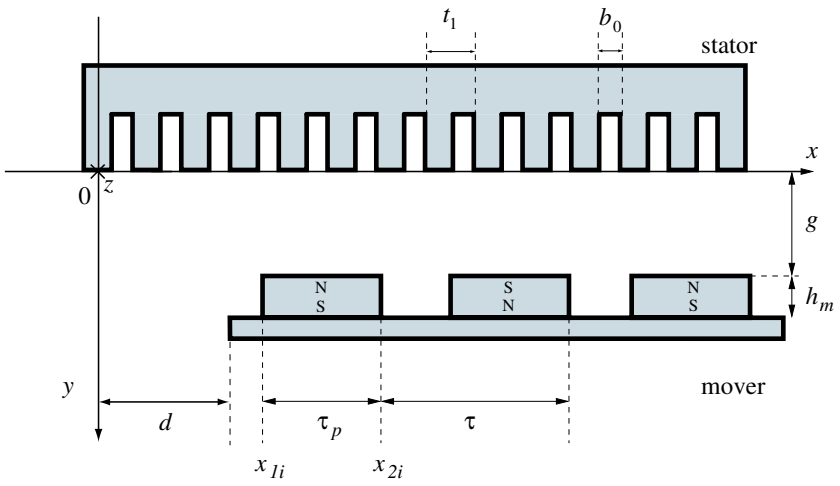

Figure 3: Inertial frame used in the analysis of a PMSLM

the *height of the magnets,* p_m the *number of permanent magnets*, g the *air-gap length*, t_1 the *slot pitch*, b_0 the *slot aperture*, τ the *permanent magnets pole pitch*, τ_p the *permanent magnets pole arc*, and σ_m the *surface magnetic charge*. In order to take into account the effect of the slots in the stator, we replace the air-gap g by the *effective air-gap* g_e, with $g_e = gK_c$, where K_c denotes *Carter's coefficient* given by

$$K_c = \frac{t_1}{t_1 - g\gamma_1},$$
$$\gamma_1 = \frac{4}{\pi}\left[\frac{b_0}{2g}\arctan\left(\frac{b_0}{2g}\right) - \ln\sqrt{1+\left(\frac{b_0}{2g}\right)^2}\right].$$

A simple calculation shows that the position of the kth image of σ_m is given by

$$h_k = \begin{cases} (k+1)h_m + kg_e & k \text{ odd} \\ kh_m + (k+1)g_e & k \text{ even} \end{cases}$$

Having found the images' positions, given an air-gap length g, the method of images yields the y component of the magnetic field intensity at a point (x_0, y_0, z_0) as follows

$$H_{pmy}(x_0, y_0, z_0, g) = \frac{\sigma_m}{4\pi}\sum_{i=1}^{p_m}\sum_{k=-\infty}^{\infty}(-1)^{k+i}\left[\arctan\frac{(x_0-x)(z_0-z)}{(y_0-h_k)D_k}\right]\Bigg|_{x=x_{2i}}^{x=x_{1i}}\Bigg|_{z=-L_A/2}^{z=L_A/2} \quad (1)$$

where

$$D_k = \sqrt{(x_0 - x)^2 + (y_0 - h_k)^2 + (z_0 - z)^2}, \quad x_{1i} = \left(i - \frac{1+\alpha}{2}\right)\tau, \quad x_{2i} = \left(i - \frac{1-\alpha}{2}\right)\tau, \quad \alpha = \frac{\tau_p}{\tau}.$$

Since a closed form for (1) cannot be found, we seek a good approximation of it on the surface of the stator, i.e., when $y_0 = 0$. To this end, we first fix the air-gap length, $g = g_0$, and then average the field intensity along the z axis. This gives the average field intensity on the stator,

$$H^{g_0}_{pmyav}(x_0, 0) = \frac{2}{L_A}\int_0^{L_A/2} H_{pmy}(x_0, y_0 = 0, z_0, g = g_0)dz_0.$$

When numerically evaluating this expression for different values of x_0, it is found that $H^{g_0}_{pmyav}$ closely resembles a sinusoid. Hence, a first order Fourier series approximation can replace $H^{g_0}_{pmyav}$ without considerable loss of accuracy. The first Fourier coefficient is given by

$$H^{g_0}_{pmy1} = \frac{4}{\tau}\int_{n\tau}^{n\tau+\tau/2} H^{g_0}_{pmyav}(x_0, 0)\sin\left(\frac{\pi}{\tau}x_0\right)dx_0,$$

where $n = \frac{p_m}{2}$ with p_m the number of poles in the mover. Next, let μ_0 be the permeability of free space. Since in the air-gap $B_{pm} = \mu_0 H_{pm}$, the approximation of the y component of the flux density due to the permanent magnets is

$$B^{g_0}_{pmy}(x_0) \simeq B^{g_0}_{pmy1}\sin\left(\frac{\pi}{\tau}x_0\right) := \mu_0 H^{g_0}_{pmy1}\sin\left(\frac{\pi}{\tau}x_0\right).$$

Recall that this expression holds for a fixed air-gap length g_0. Since levitation involves a variable air-gap length, B_{pmy} becomes a function of (x_0, g_0). We incorporate a variable air-gap by calculating the coefficient $\mu_0 H^{g_0}_{pmy1}$ for different values of g_0 over the range of interest, and performing a polynomial interpolation to obtain a function $\mu_0 H_{pmy1}(g_0)$. This gives

$$B_{pmy}(x_0, g_0) \simeq C_1(g_0)\sin\left(\frac{\pi}{\tau}x_0\right) := \mu_0 H_{pmy1}(g_0)\sin\left(\frac{\pi}{\tau}x_0\right).$$

2.2 Magnetic field produced by the stator

The stator of a PMLSM hosts three phase single layer winding producing a traveling magnetic field. Let $\mathbf{I}_a$, $\mathbf{I}_b$, and $\mathbf{I}_c$ be the phasors of the phase currents and I_a, I_b, and I_c be their magnitudes. Denote the corresponding instantaneous currents by i_a, i_b, and i_c, such that $i_a(t) \leq I_a$, $i_b(t) \leq I_b$, and $i_c(t) \leq I_c$. Let d denote *relative displacement of the mover with respect to the stator,* as illustrated in Figure 3. Let i_d and i_q denote the *direct and quadrature currents* associated with the three phase currents i_a, i_b, and i_c. Then,

we have

$$\begin{bmatrix} i_d \\ i_q \end{bmatrix} = \frac{2}{3} \begin{bmatrix} \cos(\frac{\pi}{\tau}d) & \cos\left(\frac{\pi}{\tau}d - \frac{2\pi}{3}\right) & \cos\left(\frac{\pi}{\tau}d + \frac{2\pi}{3}\right) \\ -\sin(\frac{\pi}{\tau}d) & -\sin\left(\frac{\pi}{\tau}d - \frac{2\pi}{3}\right) & -\sin\left(\frac{\pi}{\tau}d + \frac{2\pi}{3}\right) \end{bmatrix} \begin{bmatrix} i_a \\ i_b \\ i_c \end{bmatrix}$$

$$i_a + i_b + i_c = 0.$$

Further,

$$i_d = I_a \cos\left(\frac{\pi}{\tau}d\right), \quad i_q = -I_a \sin\left(\frac{\pi}{\tau}d\right).$$

Let W be the *number of turns of wire on each phase*, p the *number of pairs of poles in the stator*, w_c the *coil pitch*, and k_{w1} the *first component of the winding factor*, given by

$$k_{w1} = \frac{\sin\left(\frac{\pi}{6}\right)}{\frac{w_c}{3t_1}\sin\left(\frac{\pi t_1}{2\tau}\right)} \sin\left(\frac{\pi w_c}{2\tau}\right).$$

Following (Nasar and Xiong 1989) or (Gieras and Piech 2000), the fundamental component of the magnetomotive force is given by

$$\mathcal{F}_{s1}(x) = F_{s1} \sin\left(\frac{\pi}{\tau}x\right) = \frac{6\sqrt{2}Wk_{w1}}{\pi K_c p} I_a \sin\left(\frac{\pi}{\tau}x\right).$$

$\mathcal{F}_{s1}$ serves as boundary condition for the PDE associated with the first harmonic of the magnetic potential. The solution to such PDE yields the x and y components of the first harmonic of the magnetic flux density in the stator

$$B_{s1x}(x,y,g) = -C_2(y,g)\cos\left(\frac{\pi}{\tau}x\right) := -\mu_0 \frac{\pi}{\tau} F_{s1} \frac{\sinh\left[\frac{\pi}{\tau}(h_m + g - y)\right]}{\sinh\left[\frac{\pi}{\tau}(h_m + g)\right]} \cos\left(\frac{\pi}{\tau}x\right) \tag{2}$$

$$B_{s1y}(x,y,g) = -C_3(y,g)\sin\left(\frac{\pi}{\tau}x\right) := -\mu_0 \frac{\pi}{\tau} F_{s1} \frac{\cosh\left[\frac{\pi}{\tau}(h_m + g - y)\right]}{\sinh\left[\frac{\pi}{\tau}(h_m + g)\right]} \sin\left(\frac{\pi}{\tau}x\right).$$

2.3 Slots effect

The difference in reluctance between the slots and the teeth of the stator (see Figure 4) affects the performance of the system in two different ways (Zhu and Howe 1993). First, it attenuates the magnetic field in the air-gap, reducing the magnitude of the forces. This phenomenon is equivalent to having an effective air-gap length larger than the actual one. Second, the slots spatially modulate the field because the flux lines travel through low reluctance regions (the teeth). A magnetic model accounts for the first effect by introducing Carter's coefficient and the effective air-gap (as seen in Section 2.1) and for the second effect by calculating the *relative permeance* of the stator, derived next by adapting the results in (Zhu and Howe 1993) to PMLSMs. According to (Zhu and Howe 1993), to take into account the presence of slots,

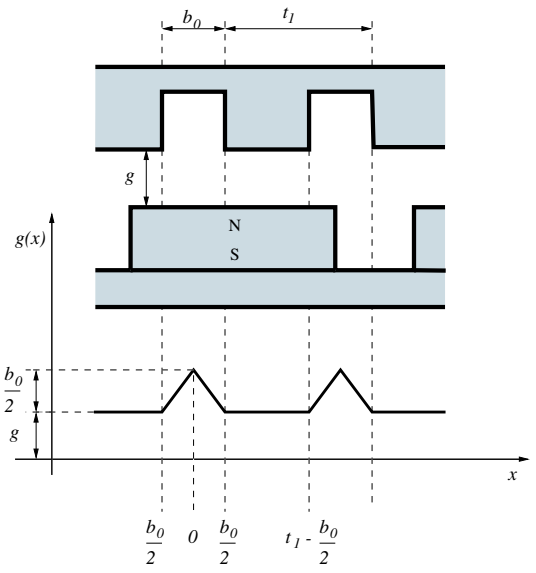

Figure 4: Modeling of the slots through the function $g(x)$

one has to modulate the magnetic field density in the airgap, $\mathbf{B}_g$, by the *relative permeance* $\tilde{\lambda}$ as follows

$$\mathbf{B}'_g = \mathbf{B}_g \tilde{\lambda},$$

where

$$\tilde{\lambda} = \frac{g + \frac{h_m}{\mu_{rec}}}{g(x) + \frac{h_m}{\mu_{rec}}},$$

and μ_{rec} is the *relative recoil permeability of the permanent magnets*. In the expression above, g is the original air-gap length and the function $g(x)$ represents the shortest distance that the flux lines have to travel through the slots before reaching the teeth when leaving the magnets from a point along the x axis (see Figure 4). In order to find an analytical expression for $g(x)$ we need the following assumption.

Assumption A1 (Geometry of the slots): The width of each slot is much greater than its depth. Thus, the magnetic flux lines travel vertically through the air-gap and horizontally inside the slots.

Using A1, elementary calculations show that

$$g(x) = \begin{cases} g + kt_1 + \frac{b_0}{2} - |x| & kt_1 - \frac{b_0}{2} \leq x \leq kt_1 + \frac{b_0}{2} \\ g & kt_1 + \frac{b_0}{2} \leq x \leq (k+1)t_1 - \frac{b_0}{2}, \end{cases}$$

where k is the index of each slot, b_0 its width and t_1 its pitch. Since $g(x)$ is a periodic and piecewise continuous function, in what follows we use the fundamental component of its Fourier expansion

$$\tilde{\lambda} \simeq 1 - \frac{b_0^2}{4t_1(g + \frac{b_0}{2} + \frac{h_m}{\mu_{rec}})}. \tag{3}$$

2.4 Forces calculation

The superposition of the permanent magnets and the winding field densities yields the resultant field density in the air-gap. After incorporating the relative permeance, the resultant field density leads to expressions for the forces in the machine. Our development follows (Nasar and Xiong 1989) but it incorporates a variable air-gap length.

2.4.1 Longitudinal Force

The longitudinal force depends on the magnetic charge and also on the x component of the traveling magnetic field in (2), which in turn is affected by the relative permeance given in (3). Given a magnetic charge σ_m distributed over a surface S, its interaction with the stator magnetic flux density produces a longitudinal force

$$F_x = \sigma_m \int_S \tilde{\lambda} B_{sx} dS,$$

where B_{sx} is the x component of B_s. Letting S be the surface of the top faces of the permanent magnets and approximating B_{sx} by its first harmonic in (2) we obtain (refer to Figure 3)

$$\begin{aligned} F_x &\simeq p_m L_A \sigma_m \int_{d+\tau/2-\frac{\tau_p}{2}}^{d+\tau/2+\frac{\tau_p}{2}} \tilde{\lambda} B_{s1x}(x, y = g, g) dx \\ &= -\frac{p_m L_A \sigma_m \mu_0 \frac{\pi}{\tau} F_{s1} \tilde{\lambda} \sinh\left(\frac{\pi}{\tau} h_m\right)}{\sinh\left(\frac{\pi}{\tau}(h_m + g)\right)} \int_{d+\tau/2-\frac{\tau_p}{2}}^{d+\tau/2+\frac{\tau_p}{2}} \cos\left(\frac{\pi}{\tau} x\right) dx \\ &= K_1(g) I_a \sin\left(\frac{\pi}{\tau} d\right) = -K_1(g) i_q, \end{aligned} \tag{4}$$

where

$$K_1(g) = 12\sqrt{2} W k_{w1} \frac{p_m L_A \sigma_m \mu_0 \tilde{\lambda} \sinh\left(\frac{\pi}{\tau} h_m\right)}{\pi K_c p \sinh\left(\frac{\pi}{\tau}(h_m + g)\right)} \sin\left(\frac{\pi \tau_p}{2\tau}\right),$$

and $\tilde{\lambda}$ is given by (3).

2.4.2 Normal force

Following (Nasar and Xiong 1989), the normal force exerted on the surface of the mover is found by using the Maxwell stress tensor

$$\mathbf{F} = \frac{1}{\mu_0} \int\limits_S \left[(\mathbf{n} \cdot \mathbf{B'_g}) \mathbf{B'_g} - \frac{B'^2_g}{2} \mathbf{n} \right] dS.$$

Here S is a rectangle lying on the plane $y = 0$ whose dimension coincides with that of the mover, $\mathbf{n}$ is its unit normal pointing in the opposite direction as the y axis, $\mathbf{B'_g}$ is the overall magnetic flux density in the airgap multiplied by the relative permeance $\tilde{\lambda}$, and B'_g is its norm. Letting B'_{gx} and B'_{gy} denote the components of $\mathbf{B'_g}$, simple calculations show that the normal component of the force is given by

$$F_y = -\frac{L_A p_m \tau}{2\mu_0} \int_0^\tau B'^2_{gy} - B'^2_{gx} dx.$$

Ideally, every flux line enters a magnet perpendicularly to its surface, so we neglect B_{gx} and obtain

$$\begin{aligned} F_y &= -\frac{L_A p_m}{2\mu_0} \int_0^\tau B'^2_{gy} d\chi \\ &= -\frac{L_A p_m}{2\mu_0} \tilde{\lambda} \int_0^\tau \left\{ C_1(g) \sin\left(\frac{\pi}{\tau}\chi\right) - C_3(0,g) \sin\left[\frac{\pi}{\tau}(\chi + d)\right] \right\}^2 d\chi \\ &= -\frac{L_A p_m \tau}{4\mu_0} \tilde{\lambda} \left[C_1(g)^2 + C_3(0,g)^2 - 2C_1(g)C_3(0,g) \cos\left(\frac{\pi}{\tau} d\right) \right] \\ &= -\left[K_2(g) + K_3(g) i_d + K_4(g)(i_d^2 + i_q^2) \right], \end{aligned} \tag{5}$$

where

$$\begin{aligned} K_2(g) &= \tilde{\lambda} \frac{L_A p_m \tau \mu_0}{4} H_{pmy1}(g)^2 \\ K_3(g) &= -\tilde{\lambda} \frac{3\sqrt{2} L_A p_m W k_{w1} \mu_0}{K_c p} H_{pmy1}(g) \coth\left[\frac{\pi}{\tau}(h_m + g)\right] \\ K_4(g) &= \tilde{\lambda} \frac{18 L_A p_m W^2 k_{w1}^2 \mu_0}{\tau K_c^2 p^2} \coth^2\left[\frac{\pi}{\tau}(h_m + g)\right]. \end{aligned}$$

3 The model of the three degrees of freedom system

We are now ready to develop a model for the system depicted in Figure 1. The system employs three identical motors equally spaced along a straight line and perpendicularly oriented with respect to each other. The windings of motors 1 and 3 (those at the ends of the structure) are connected in series whereas motor 2 is independently fed. In order to allow for a large range of operation, the movers of the motors are significantly smaller than their stators. In addition to the previous specifications, the design takes into account the following constraints.

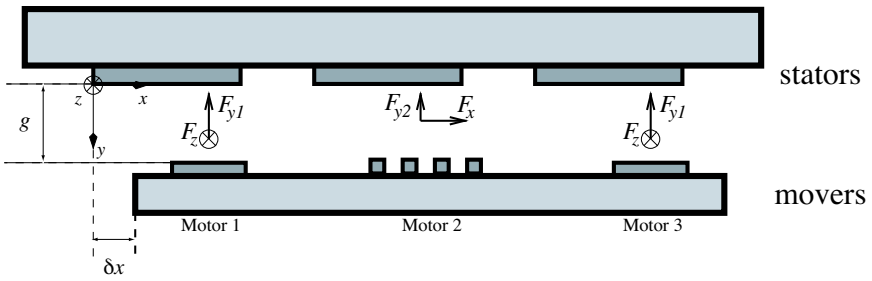

Figure 5: Forces in the three-PMLSMs configuration

Assumption A2 (Magnetic fields interaction): The motors are placed sufficiently far from each other so that their fields do not interfere.

Assumption A3 (Rotational degrees of freedom): The platen is not allowed to rotate.

This assumption can be removed if one controls the roll and pitch of the platen. To do that, a different setup than the one displayed in Figure 1 is needed and a minor variation of the technique presented in Section 4.2 can be employed to control the resulting five DOF. We will not dwell on this topic any further in this paper.

Let M_{pm} be the *mass of each permanent magnet*, M_t *the mass of the platen* without permanent magnets, M_{bi} the *mass of each back iron*, and M_p the *total mass of the platen.* The mass of the platen is then given by

$$M_p = M_t + 3p_m M_{pm} + 3M_{bi}.$$

Let Motor 1 and Motor 3 be the ones generating thrust along the z axis and Motor 2 the one generating thrust along the x axis (see Figure 5). Let also i_{d1} and i_{q1} be the direct and quadrature currents fed to Motors 1 and 3. Similarly, let i_{d2} and i_{q2} be the direct and quadrature currents through the windings of Motor 2. Let δx and δz denote the *horizontal displacements of the platen,* and g denote the *airgap.* If the forces on the motors are defined as in Figure 5, Newton's law yields the following equations

$$\begin{aligned} M_p\ \ddot{g} &= M_p G + 2F_{y1}(g, i_{d1}, i_{q1}) + F_{y2}(g, i_{d2}, i_{q2}) \\ M_p\ \ddot{\delta x} &= F_x(g, i_{q2}) \\ M_p\ \ddot{\delta z} &= 2F_z(g, i_{q1}) \end{aligned}$$

where G is the gravitational acceleration, $F_{y1}(g, i_{d1}, i_{q1})$ and $F_z(g, i_{q1})$ are the forces exerted by Motor 1 and 3, and $F_{y2}(g, i_{d2}, i_{q2})$ and $F_x(g, i_{q2})$ are the forces exerted by Motor 2. These forces are given by

expressions (4) and (5). Letting

$$\mathbf{x} = [g, \dot{g}, \delta x, \dot{\delta x}, \delta z, \dot{\delta z}]^\top, \ u = [i_{q1}, i_{q2}, i_{d1}, i_{d2}]^\top$$

we get the state space model

$$\begin{aligned}
\dot{x}_1 &= x_2 \\
\dot{x}_2 &= G - L_4(x_1)[2u_1^2 + u_2^2 + 2u_3^2 + u_4^2] - L_3(x_1)[2u_3 + u_4] - 3L_2(x_1) \\
\dot{x}_3 &= x_4 \\
\dot{x}_4 &= -L_1(x_1)u_2 \\
\dot{x}_5 &= x_6 \\
\dot{x}_6 &= -2L_1(x_1)u_1.
\end{aligned} \tag{6}$$

where $L_i(x_1) := \dfrac{K_i(x_1)}{M_p}$, $i = 1, \ldots, 4$.

4 Nonlinear Control Design

In this section we investigate the set-point stabilization problem for system (6) through two nonlinear approaches.

4.1 Lyapunov-Based Design

Let $\mathbf{x}^d = [x_1^d, 0, x_2^d, 0, x_3^d, 0]^\top$ be the desired set-point and define

$$\tilde{\mathbf{x}} = \mathbf{x} - \mathbf{x}^d, \ \tilde{\mathbf{x}}^1 = [\tilde{x}_1, \tilde{x}_2]^\top, \ \tilde{\mathbf{x}}^2 = [\tilde{x}_3, \ldots, \tilde{x}_6]^\top.$$

Next, consider the controller

$$\begin{aligned}
\begin{bmatrix} u_1 \\ u_2 \end{bmatrix} &= \begin{bmatrix} 0 & -\frac{1}{2L_1(x_1)} \\ -\frac{1}{L_1(x_1)} & 0 \end{bmatrix} \begin{bmatrix} v_1(\tilde{\mathbf{x}}^2) \\ v_2(\tilde{\mathbf{x}}^2) \end{bmatrix} \\
u_3 &= 0 \\
u_4 &= -\frac{L_3(x_1) + \sqrt{R(\tilde{\mathbf{x}})}}{2L_4(x_1)}
\end{aligned} \tag{7}$$

where

$$\begin{aligned}
R(\tilde{\mathbf{x}}) &= [L_3(x_1)]^2 + 4L_4(x_1)\Big[\tilde{\epsilon}\,(\tilde{x}_1 + \tilde{x}_2)\,(\tilde{x}_1^2 + \tilde{x}_2^2) + \tilde{x}_2 - L_4(x_1)U(\tilde{\mathbf{x}}) + G - 3L_2(x_1)\Big] \\
\begin{bmatrix} v_1(\tilde{\mathbf{x}}^2) \\ v_2(\tilde{\mathbf{x}}^2) \end{bmatrix} &= -K\tilde{\mathbf{x}}^2, \quad U(\tilde{\mathbf{x}}) = 2\left(\frac{v_2(\tilde{\mathbf{x}}^2)}{2L_1(x_1)}\right)^2 + \left(\frac{v_1(\tilde{\mathbf{x}}^2)}{L_1(x_1)}\right)^2,
\end{aligned} \tag{8}$$

K is a 2×4 matrix and $\tilde{\epsilon} > 0$. The controller above is well-defined on the set

$$\mathcal{D} = \{(\tilde{\mathbf{x}}^1, \tilde{\mathbf{x}}^2) \in \mathbb{R}^2 \times \mathbb{R}^4 : R(\tilde{\mathbf{x}}) \geq 0, L_4(x_1) \neq 0, L_1(x_1) \neq 0\},$$

and the closed-loop system reads as

$$\tilde{\mathbf{x}}^1 \quad : \quad \begin{cases} \dot{\tilde{x}}_1 = \tilde{x}_2 \\ \dot{\tilde{x}}_2 = -\tilde{\epsilon}\,(\tilde{x}_1 + \tilde{x}_2)\,[\tilde{x}_1^2 + \tilde{x}_2^2] - \tilde{x}_2 \end{cases} \tag{9}$$

$$\dot{\tilde{\mathbf{x}}}^2 \quad = \quad (A_c - B_c K)\tilde{\mathbf{x}}^2. \tag{10}$$

where the pair (A_c, B_c) is in Brunovsky normal form. Choose K so that $A_c - B_c K$ is Hurwitz. Clearly, if $L_1(x_1) \neq 0$, u_1 and u_2 are well-defined and the $\tilde{\mathbf{x}}^2$ subsystem is exponentially stable. Let P be the positive definite matrix satisfying

$$(A_c - B_c K)^\top P + P(A_c - B_c K) = -I,$$

so that, letting $V^2 = \tilde{\mathbf{x}}^{2\top} P \tilde{\mathbf{x}}^2$, the set $\Omega_d^2 = \{\tilde{\mathbf{x}}^2 : V^2(\tilde{\mathbf{x}}^2) \leq d\}$ is positively invariant for any $d \geq 0$. Next, consider the Lyapunov function candidate $V^1(\tilde{\mathbf{x}}^1) = \frac{1}{2}\tilde{x}_1^2 + \frac{1}{2}(\tilde{x}_1 + \tilde{x}_2)^2$ whose derivative is given by

$$\begin{aligned} \dot{V}^1(\tilde{\mathbf{x}}^1) &= -\tilde{x}_1^2 + \tilde{x}_1(\tilde{x}_1 + \tilde{x}_2) - \tilde{\epsilon}(\tilde{x}_1 + \tilde{x}_2)^2[\tilde{x}_1^2 + \tilde{x}_2^2] \\ &\leq -\frac{\tilde{x}_1^2}{2} - \left\{\tilde{\epsilon}\left[\tilde{x}_1^2 + \tilde{x}_2^2\right] - \frac{1}{2}\right\}(\tilde{x}_1 + \tilde{x}_2)^2. \end{aligned}$$

$\dot{V}^1(\tilde{\mathbf{x}}^1)$ is negative outside the ball $D = \left\{\tilde{\mathbf{x}}^1 \in \mathbb{R}^2 : \tilde{x}_1^2 + \tilde{x}_2^2 \leq \frac{1}{2\tilde{\epsilon}}\right\}$. Let

$$\Omega_d^1 = \{\tilde{\mathbf{x}}^1 \in \mathbb{R}^2 : V^1(\tilde{\mathbf{x}}^1) \leq d\}$$

and notice that $d^* = \frac{3+\sqrt{5}}{8\tilde{\epsilon}}$ is the smallest real number guaranteeing that $D \subset \Omega_d^1$. In other words,

$$V^1 \geq d^* \Rightarrow \dot{V}^1 \leq 0,$$

and thus Ω_d^1 is positively invariant for all $d \geq d^*$.

Consider now the function $W(\tilde{\mathbf{x}}^1) = \frac{(\tilde{x}_1 + \tilde{x}_2)^2}{2}$, then

$$\dot{W}(\tilde{\mathbf{x}}^1) = -\tilde{\epsilon}(\tilde{x}_1 + \tilde{x}_2)^2(\tilde{x}_1^2 + \tilde{x}_2^2) \leq 0, \forall \tilde{\mathbf{x}}^1 \in \mathbb{R}^2.$$

Let $E = \{\tilde{\mathbf{x}}^1 \in \Omega_d^1 : \dot{W}(\tilde{\mathbf{x}}^1) = 0\} = \{\tilde{\mathbf{x}}^1 \in \Omega_d^1 : (\tilde{x}_1 + \tilde{x}_2) = 0\}$. For any trajectory in E, the dynamics of

(9) are given by

$$\begin{aligned} \dot{\tilde{x}}_1 &= -\tilde{x}_1 \\ \dot{\tilde{x}}_2 &= -\tilde{x}_2. \end{aligned} \tag{11}$$

Hence, on E, $\dot{\tilde{x}}_1 + \dot{\tilde{x}}_2 = 0$, showing that E is invariant. Applying LaSalle's theorem, we conclude that, for all $d \geq d^*$, every integral curve of (9) leaving from Ω_d^1 approaches E as $t \to \infty$. Moreover, from (11), $\tilde{x}_1 \to 0$ on E. Since Ω_d^1 is compact, all trajectories are bounded and it follows that, for all $\tilde{\mathbf{x}}^1(0) \in \Omega_d^1$, $\tilde{\mathbf{x}}^1(t) \to 0$. Again, this holds for all d such that $d > d^*$.

We now seek to find an estimate of the domain of attraction of the origin $\tilde{\mathbf{x}} = 0$. This can be accomplished, in principle, by numerically finding the largest real numbers d_1 and d_2 such that

$$\Omega_{d_1}^1 \times \Omega_{d_2}^2 \subset \mathcal{D} = \{(\tilde{\mathbf{x}}^1, \tilde{\mathbf{x}}^2) \in \mathbb{R}^2 \times \mathbb{R}^4 : R(\tilde{\mathbf{x}}) \geq 0, L_4(x_1) \neq 0, L_1(x_1) \neq 0\},$$

but this is computationally too hard. The problem can be significantly simplified by finding an upper bound to $R(\tilde{\mathbf{x}})$ in (8) which depends only on $\tilde{\mathbf{x}}^1$. If that can be done, the estimation of the domain of attraction can be easily carried out numerically on the $(\tilde{x}_1, \tilde{x}_2)$ plane. From (8), it is clear that finding an upper bound to

$$\ell(\tilde{\mathbf{x}}^2) = v_1(\tilde{\mathbf{x}}^2)^2 + \frac{v_2(\tilde{\mathbf{x}}^2)^2}{2}$$

gives a lower bound on $R(\tilde{\mathbf{x}})$ which depends only on $\tilde{\mathbf{x}}^1$. Assume that $\tilde{\mathbf{x}}^2(0) \in \Omega_{d_2}^2$, for some $d_2 > 0$, so that $\tilde{\mathbf{x}}^2(t) \in \Omega_{d_2}^2$ for all $t \geq 0$. Recall that $[v_1, v_2]^\top = -K\tilde{\mathbf{x}}^2$, where K is a 2×4 matrix, and let $K' = diag[1, 1/\sqrt{2}]K$. Then, $\ell(\tilde{\mathbf{x}}^2) = \tilde{\mathbf{x}}^{2\top} K'^\top K' \tilde{\mathbf{x}}^2$ and its upper bound is given by

$$\max_{\Omega_{d_2}^2} \left\{ \tilde{\mathbf{x}}^{2\top} K'^\top K' \tilde{\mathbf{x}}^2 \right\} = \max_{\{\tilde{\mathbf{x}}^{2\top} P \tilde{\mathbf{x}}^2 \leq d_2\}} \left\{ \tilde{\mathbf{x}}^{2\top} K'^\top K' \tilde{\mathbf{x}}^2 \right\}.$$

This constrained optimization problem can be solved analytically. From the Khun-Tucker necessary conditions we have that extrema are either points in the interior of $\Omega_{d_2}^2$ such that $\nabla \ell = 0$, i.e.,

$$K'^\top K' \tilde{\mathbf{x}}^2 = 0 \iff \tilde{\mathbf{x}}^2 \in \ker(K'^\top K'),$$

for which $\ell(\tilde{\mathbf{x}}^2) = 0$, or points on the boundary of $\Omega_{d_2}^2$ such that $\nabla \ell$ is parallel to the gradient of the constraint, i.e.,

$$\text{(i) } K'^\top K' \tilde{\mathbf{x}}^2 = \lambda P \tilde{\mathbf{x}}^2 \iff (K'^\top K' - \lambda P)\tilde{\mathbf{x}}^2 = 0$$

$$\text{(ii) } \tilde{\mathbf{x}}^{2\top} P \tilde{\mathbf{x}}^2 = d_2,$$

for some real number λ. Using the Cholesky decomposition of P, $P = LL^\top$, with L invertible, condition

(i) can be rewritten as

$$\begin{aligned}(K'^{\top}K' - \lambda P)\tilde{\mathbf{x}}^2 = 0 &\iff (K'^{\top}K - \lambda LL^{\top})\tilde{\mathbf{x}}^2 = 0 \\ &\iff (L^{-1}K'^{\top}K'L^{-\top} - \lambda I)L^{\top}\tilde{\mathbf{x}}^2 = 0.\end{aligned}$$

Hence, for condition (i) to be satisfied, λ must be an eigenvalue of $L^{-1}K'^{\top}K'L^{-\top}$ (or, equivalently, an eigenvalue of $P^{-1}K'^{\top}K'$) and, letting v be the eigenvector associated to λ with $\|v\| = 1$, $\tilde{\mathbf{x}}^2$ must solve $L^{\top}\tilde{\mathbf{x}}^2 = \mu v$, for some real number μ. So one must have $\tilde{\mathbf{x}}^2 = \mu L^{-\top}v$. Notice that all eigenvalues of $L^{-1}K'^{\top}K'L^{-\top}$ are real and nonnegative.

Next, for condition (ii) to be satisfied, one must have

$$\begin{aligned}\mu^2 v^{\top}L^{-1}PL^{-\top}v = d_2 &\iff \mu^2 v^{\top}L^{-1}(LL^{\top})L^{-\top}v = d_2 \\ &\iff \mu^2 = d_2.\end{aligned}$$

Then, the corresponding value of ℓ is

$$\begin{aligned}\ell(\tilde{\mathbf{x}}^2) = \ell(\mu L^{-\top}v) &= d_2 v^{\top}(L^{-1}K'^{\top}K'L^{-\top}v) \\ &= d_2 v^{\top}(\lambda v) \\ &= d_2\lambda.\end{aligned}$$

In conclusion, the maximum value of ℓ is given by

$$\max_{\Omega^2_{d_2}} \ell(\tilde{\mathbf{x}}^2) = \max\left\{0, d_2\,\lambda_{max}(L^{-1}K'^{\top}K'L^{-\top})\right\} = d_2\,\lambda_{max}(P^{-1}K'^{\top}K'). \tag{12}$$

This result is used in the following procedure to determine an estimate of the domain of attraction of $\tilde{\mathbf{x}} = 0$.

Procedure 1: Estimation of the domain of attraction of $\tilde{\mathbf{x}} = 0$

1. Numerically find the set $\mathcal{X}_1 = \{x_1 : L_3(x_1)^2 + 4L_4(x_1)(G - 3L_2(x_1)) > 0,\ L_4(x_1) \neq 0,\ L_1(x_1) \neq 0\}$
2. Choose the set point for the air-gap in this set, i.e., choose $x_1^d \in \mathcal{X}_1$
3. Choose $K \in \mathbb{R}^{2\times 4}$ such that the pair $A_c - B_c K$ is Hurwitz
4. Set $U^* = \left(\frac{L_1(x_1^d)}{2L_4(x_1^d)}\right)^2 \left(L_3(x_1^d)^2 + 4L_4(x_1^d)G - 12L_4(x_1^d)L_2(x_1^d)\right)$, and choose $\hat{U} \in (0, U^*)$. Find the feasible horizontal operating range for the platen:
   (a) Let $K' = diag[1, 1/\sqrt{2}]K$
   (b) Set $d_2 = \hat{U}/\lambda_{max}(P^{-1}K'^{\top}K')$. The horizontal operating range is $\tilde{\mathbf{x}}^2 \in \Omega_{d_2}^2$
5. Choose $\tilde{\epsilon} > 0$ in (8) and find (possibly the largest) $d_1 > 0$ such that

$$\Omega_{d_1} \subset \hat{\mathcal{D}} = \{\tilde{\mathbf{x}}^1 \in \mathbb{R}^2 : \hat{R}(\tilde{\mathbf{x}}^1) \geq 0, L_4(x_1) \neq 0, L_1(x_1) \neq 0\}$$
$$\hat{R}(\tilde{\mathbf{x}}^1) = L_3(x_1)^2 + 4L_4(x_1)\left(\tilde{\epsilon}\,(\tilde{x}_1 + \tilde{x}_2)\,(\tilde{x}_1^2 + \tilde{x}_2^2) + \tilde{x}_2 - \frac{L_4(x_1)}{[L_1(x_1)]^2}\hat{U} + G - 3L_2(x_1)\right)$$

6. Check whether $\tilde{\epsilon} \geq \frac{2+\sqrt{5}}{8d_1}$. If not, repeat item 5 with some other choice of $\tilde{\epsilon}$. If yes, the feasible vertical operating range for the platen is $\tilde{\mathbf{x}}^1 \in \Omega_{d_1}^1$

Lemma 1 *Let x_1^d be any point in the set $\mathcal{X}_1$ defined in item 1 of the procedure. If there exists $\tilde{\epsilon}$ satisfying the requirement in item 6, then any integral curve of the closed-loop system (6), (7) leaving from a point in the set $\Omega_{d_1}^1 \times \Omega_{d_2}^2$ is bounded and asymptotically approaches the equilibrium $\mathbf{x} = \mathbf{x}^d$.*

Remark 1: Note that the result in Lemma 1 guarantees boundedness of $\mathbf{x}$ and attractiveness of the equilibrium $\mathbf{x}^d$, but not Lyapunov stability.

Proof of Lemma 1: We primarily need to show that every integral curve of (9), (10) leaving from $\Omega_{d_1}^1 \times \Omega_{d_2}^2$, with d_1 and d_2 defined in the procedure above, is entirely contained in the set $\mathcal{D}$. By the choice of x_1^d, U^* defined in item 4 of the procedure is such that

$$\Psi(U^*) \triangleq L_3(x_1)^2 + 4L_4(x_1)\left(-\frac{L_4(x_1^d)}{[L_1(x_1^d)]^2}U^* + G - 3L_2(x_1)\right) = 0.$$

Since $L_4(x_1^d) \neq 0$ and $L_1(x_1^d) \neq 0$, for any $\hat{U} \in (0, U^*)$ we have $\Psi(\hat{U}) > 0$. Thus, for all $x_1^d \in \mathcal{X}_1$ and all $\hat{U} \in (0, U^*)$, $\hat{R}([0\ 0]^{\top}) > 0$, implying that $\Omega_0^1 \subset \operatorname{int}\hat{\mathcal{D}}$. By the continuity of $\hat{R}(\cdot)$, $L_4(\cdot)$, and $L_1(\cdot)$, there exists a positive real number d_1 satisfying the requirement in item 5 of the procedure. By the definition of

d_2 in item 4, the set $\Omega^2_{d_2}$ is positively invariant and

$$\max_{\Omega^2_{d_2}} \left(v_1^2 + \frac{v_2^2}{2} \right) = \hat{U}.$$

Thus, for any $\tilde{\mathbf{x}}^2(0) \in \Omega^2_{d_2}$, $R(\tilde{\mathbf{x}}(t)) \geq \hat{R}(\tilde{\mathbf{x}}^1(t))$. If $\tilde{\epsilon}$ satisfies item 6 of the procedure, then $d_1 \geq \frac{3+\sqrt{5}}{8\tilde{\epsilon}}$, implying that $\Omega^1_{d_1}$ is positively invariant. Thus we obtain

$$\begin{aligned} \tilde{\mathbf{x}}^1(0) \in \Omega^1_{d_1} \text{ and } \tilde{\mathbf{x}}^2(0) \in \Omega^2_{d_2} &\Rightarrow \tilde{\mathbf{x}}^1(t) \in \hat{\mathcal{D}} \ \forall t \geq 0 \\ &\Rightarrow \tilde{\mathbf{x}}(t) \in \mathcal{D} \ \forall t \geq 0. \end{aligned}$$

In conclusion, if $\tilde{\mathbf{x}}(0) \in \Omega^1_{d_1} \times \Omega^2_{d_2}$, the controller (7) is well-defined for all $t \geq 0$ and the solution $\tilde{\mathbf{x}}(t)$ approaches the origin. ■

Remark 2: The procedure outlined above can easily be implemented numerically, as it requires studying the sign of a function over the real line (item 1) and one function over the plane (item 5). Note, however, that we do not provide an algorithm to choose $\tilde{\epsilon}$. The simulations in Section 5.1 indicate that there is a wide range of values of $\tilde{\epsilon}$ satisfying the requirement in item 6.

4.2 Dynamic Feedback Linearization

The main drawback of the control design presented in the previous section is that the size of the domain of attraction of the equilibrium $\mathbf{x}^d$ depends on the choice of x_1^d (but it does not depend on the choice of x_3^d and x_5^d). In practice it is desirable to have a guaranteed range of operation which is independent of the set point. To address this problem, we replace the function $R(\tilde{\mathbf{x}})$ in (7) by the following dynamic feedback linearizing controller

$$\begin{aligned} R(\tilde{\mathbf{x}}, z) &= L_3(x_1)^2 + 4L_4(x_1)\left(-z - L_4(x_1)U(\tilde{\mathbf{x}}) + G - 3L_2(x_1)\right) \\ \dot{z} &= -k_1\tilde{x}_1 - k_2\tilde{x}_2 - k_3 z, \end{aligned} \tag{13}$$

with $U(\cdot)$ defined as in (8). With this choice, the closed-loop dynamics read as

$$\tilde{\mathbf{x}}^1 \quad : \quad \begin{cases} \dot{\tilde{x}}_1 = \tilde{x}_2 \\ \dot{\tilde{x}}_2 = z \\ \dot{z} = -k_1\tilde{x}_1 - k_2\tilde{x}_2 - k_3 z \end{cases} \tag{14}$$

$$\tilde{\mathbf{x}}^2 \quad : \quad \tilde{\mathbf{x}}^2 = (A_c - B_c K)\tilde{\mathbf{x}}^2, \tag{15}$$

where k_1, k_2, k_3 are chosen so that the matrix

$$A = \begin{bmatrix} 0 & 1 & 0 \\ 0 & 0 & 1 \\ -k_1 & -k_2 & -k_3 \end{bmatrix}$$

is Hurwitz. As before, the vector field (14), (15) is well-defined as long as

$$(\tilde{\mathbf{x}}(t), z) \in \mathcal{D} = \{(\tilde{\mathbf{x}}, z) \in \mathbb{R}^6 \times \mathbb{R} : R(\tilde{\mathbf{x}}, z) \geq 0, L_4(x_1) \neq 0, L_1(x_1) \neq 0\}.$$

By using a dynamic feedback we ensure that $R(\tilde{\mathbf{x}}, z)$ does not directly depend on u, which makes it possible to find an estimate of the domain of attraction of the closed-loop system independently of x_1^d. To this end, we adapt the idea developed in the previous section and define the inner approximation to the projection of $\mathcal{D}$ onto the (x_1, x_2, z) coordinates

$$\hat{\mathcal{D}} = \left\{(x_1, x_2, z) \in \mathbb{R}^3 : \hat{R}(x_1, x_2, z) \geq 0, L_4(x_1) \neq 0, L_1(x_1) \neq 0\right\}$$
$$\hat{R}(x_1, x_2, z) = L_3(x_1)^2 + 4L_4(x_1)\left(-z - \frac{L_4(x_1)}{[L_1(x_1)]^2}\hat{U} + G - 3L_2(x_1)\right).$$

Similarly to what we had earlier, letting $d_2 = \hat{U}/\lambda_{max}(P^{-1}K'^{\top}K')$, the following holds

$$(x_1, x_2, z) \in \hat{\mathcal{D}} \text{ and } \tilde{\mathbf{x}}^2 \in \Omega_{d_2}^2 \Rightarrow \tilde{\mathbf{x}} \in \mathcal{D},$$

hence, to guarantee that (14), (15) are well-defined, we need to design a controller for (14) guaranteeing that $(x_1(t), x_2(t), z(t)) \in \hat{\mathcal{D}}$ for all $t \geq 0$ and $(\tilde{x}_1(t), \tilde{x}_2(t)) \to 0$.

Let H be a 3×3 positive definite matrix, C be a 3×1 vector, and R a positive real number such that the ellipsoid centered at C

$$\mathcal{N} = \left\{(x_1, x_2, z) \in \mathbb{R}^3 : [x_1 - C_1 \; x_2 - C_2 \; z - C_3]H[x_1 - C_1 \; x_2 - C_2 \; z - C_3]^{\top} \leq R\right\} \tag{16}$$

is contained in $\hat{\mathcal{D}}$. Letting $\xi = (\tilde{x}_1 + x_1^d - C_1, \tilde{x}_2 - C_2, z - C_3)$, $\mathcal{N}$ is expressed in $(\tilde{x}_1, \tilde{x}_2, z)$ coordinates as

$$\mathcal{N} = \left\{(\tilde{x}_1, \tilde{x}_2, z) \in \mathbb{R}^3 : \xi^{\top}H\xi \leq R\right\}.$$

For a choice of x_1^d, k_1, k_2, and k_3, the next lemma gives necessary and sufficient conditions for $\mathcal{N}$ to be positively invariant.

Lemma 2 *Let S denote the symmetric part of HA, i.e., $S = (HA + A^\top H)/2$, and $b = \frac{1}{2}HA[x_1^d - C_1 \ -C_2 \ -C_3]^\top$. Then $\mathcal{N}$ is positively invariant* if and only *if either of the following holds*

(i) For all λ_i $(i = 1, 2, 3)$ eigenvalues of $H^{-1}S$,

$$b \notin \text{Range}(S - \lambda_i H),$$

and the following inequality holds

$$\ell_1(\bar{\lambda}) = \bar{\lambda}R - b^\top (S - \bar{\lambda}H)^{-1} b \leq 0, \tag{17}$$

where $\bar{\lambda}$ is the largest root of

$$b^\top (S - \lambda H)^{-1} H (S - \lambda H)^{-1} b - R = 0. \tag{18}$$

(ii) For some λ_{i^*} eigenvalue(s) of $H^{-1}S$ the following properties hold

(a) $b \neq 0$ and $b \in \text{Range}(S - \lambda_{i^*} H)$

(b) Letting x be a solution to

$$(S - \lambda_{i^*} H)x = b, \tag{19}$$

there exists $y \in \ker(S - \lambda_{i^*} H)$ such that $(x + y)^\top H (x + y) = R$

(c) Letting $\ell_2(\lambda_{i^*}) = \lambda_{i^*} R - b^\top x$, $\max\{\ell_1(\bar{\lambda}), \ell_2(\lambda_{i^*})\} \leq 0$

(iii) $b = 0$ and S is negative semidefinite

Proof: $\mathcal{N}$ is positively invariant if and only if the derivative of $\xi^\top H \xi$ along the vector field (14) is negative on points of the boundary $\partial\mathcal{N}$, i.e., $\xi^\top HA[\tilde{x}_1 \ \tilde{x}_2 \ z]^\top \leq 0$ on $\{(\tilde{x}_1, \tilde{x}_2, z) : \xi^\top H \xi = R\}$. Since

$$\xi^\top HA[\tilde{x}_1 \ \tilde{x}_2 \ z]^\top = \xi^\top S \xi - 2b^\top \xi,$$

positive invariance can be checked by formulating the following *quadratically constrained quadratic programming* (QCQP) problem,

$$\begin{aligned} &\text{maximize } \xi^\top S \xi - 2b^\top \xi \\ &\text{subject to } \xi^\top H \xi = R. \end{aligned} \tag{20}$$

The Lagrange multiplier condition for this program is

$$\begin{aligned} &S\xi - b - \lambda H\xi = 0 \iff (S-\lambda H)\xi = b \\ &\xi^\top H\xi = R. \end{aligned} \tag{21}$$

If $b \notin \text{Range}(S-\lambda_i H)$ and $\lambda \neq \lambda_i$, $i=1,2,3$, then the solution to the first equation is $\xi^* = (S-\lambda H)^{-1}b$. Substituting ξ^* in the second equation we obtain (18). Substituting ξ^* in the cost function and using (18) we obtain

$$\begin{aligned} &b^\top (S-\lambda H)^{-1} S (S-\lambda H)^{-1} b - 2b^\top (S-\lambda H)^{-1} b \\ &\quad = b^\top (S-\lambda H)^{-1}(S-\lambda H+\lambda H)(S-\lambda H)^{-1} b - 2b^\top (S-\lambda H)^{-1} b \\ &\quad = b^\top (S-\lambda H)^{-1} b + \lambda b^\top (S-\lambda H)^{-1} H (S-\lambda H)^{-1} b - 2b^\top (S-\lambda H)^{-1} b \\ &\quad = \ell_1(\lambda). \end{aligned}$$

The restriction of $\ell_1(\lambda)$ to points $\lambda \in \mathbb{R}$ satisfying (18) is strictly increasing. Hence its maximum is achieved at the largest root of (18), $\bar{\lambda}$. Positive invariance of $\mathcal{N}$ is achieved if and only if $\ell_1(\bar{\lambda}) \leq 0$.

If $\lambda = \lambda_i$, for some $i = 1,2,3$, and $b \notin \text{Range}(S-\lambda_i H)$ then the first equation in (21) does not have a solution. We have thus proved part (i) of the lemma.

If, for some λ_{i^*} eigenvalue(s) of $H^{-1}S$, $b \neq 0$ and $b \in \text{Range}(S-\lambda_{i^*}H)$, there exists a 3×1 vector x satisfying (19). Then, any vector $x+y$, with $y \in \ker(S-\lambda_{i^*}H)$, solves the first equation in (21) with $\lambda = \lambda_{i^*}$. The second equation in (21) is satisfied if and only if there exists y so that $(x+y)^\top H(x+y) = R$. If that is the case, the cost associated with this extremum is

$$\begin{aligned} &(x+y)^\top S(x+y) - 2b^\top (x+y) \\ &\quad = (x+y)^\top (S-\lambda_{i^*}H)(x+y) + \lambda_{i^*}(x+y)^\top H(x+y) - 2b^\top (x+y) \\ &\quad = (x+y)^\top b + \lambda_{i^*} R - 2b^\top (x+y) \\ &\quad = \lambda_{i^*} R - b^\top x = \ell_2(\lambda_{i^*}), \end{aligned}$$

where the last identity comes from the fact that $S-\lambda_{i^*}H$ is symmetric and thus

$$b \in \text{Range}(S-\lambda_{i^*}H),\ y \in \ker(S-\lambda_{i^*}H) \Rightarrow b^\top y = 0.$$

On the other hand, from the proof of part (i) it is clear that, when $\lambda \neq \lambda_{i^*}$, extrema of the cost have value $\ell_1(\bar{\lambda})$. Thus $\mathcal{N}$ is positively invariant if and only if $\max\{\ell_1(\bar{\lambda}), \ell_2(\lambda_{i^*})\} \leq 0$, proving part (ii).

Finally, when $b=0$, (21) has a solution if and only if $\lambda = \lambda_i$, $i=1,2,3$. In this case the solution is

$\xi^* = \mu v$, where $v \in \ker(S - \lambda_i H)$ and $\mu = \sqrt{\frac{R}{v^\top H v}}$. The associated cost is

$$\begin{aligned}\xi^{*\top} S \xi^* =& R\frac{v^\top S v}{v^\top H v} = \frac{R}{v^\top H v}\left\{v^\top (S - \lambda_i H)v + \lambda_i v^\top H v\right\} \\ =& \lambda_i v, \quad i = 1, 2, 3.\end{aligned}$$

Hence $\mathcal{N}$ is positively invariant if and only if $H^{-1}S$ is negative semidefinite. Letting $H = LL^\top$ be the Cholesky decomposition of H, the eigenvalues of $H^{-1}S$ coincide with the eigenvalues of $L^{-1}SL^{-\top}$, which are negative if and only if the eigenvalues of S are negative. ■

The next lemma gives further insight to the requirement that $\mathcal{N}$ be positively invariant.

Lemma 3 *Let $\lambda^+ = \lambda_{max}(H^{-1}S)$. If $b \notin \text{Range}(S - \lambda^+ H)$, then $\mathcal{N}$ is positively invariant* only if *S is negative definite.*

Proof: Consider equation (18). It is fairly easy to show that, since $b \notin \text{Range}(S - \lambda^+ H)$,

$$\lim_{\lambda \to \lambda^+} \left\|(S - \lambda)^{-1} b\right\| = +\infty.$$

Hence, since H is positive definite, we have that

$$\lim_{\lambda \to \lambda^+} b^\top (S - \lambda H)^{-1} H (S - \lambda H)^{-1} b - R = +\infty.$$

Further, it is clear that $\lim_{\lambda \to +\infty}(S - \lambda H)^{-1} b = 0$ (to see that, use Kramer's rule for matrix inversion), and thus

$$\lim_{\lambda \to +\infty} b^\top (S - \lambda H)^{-1} H (S - \lambda H)^{-1} b - R = -R.$$

Hence, by continuity, there exists $\bar{\lambda} > \lambda^+$ such that (18) is satisfied. This shows that *the largest root of (18) is strictly larger than λ^+.*

We next show that for $\ell_1(\bar{\lambda}) < 0$ it is necessary that $\bar{\lambda} < 0$. This follows from the fact that, in (17), $S - \bar{\lambda} H$ is negative definite, implying that $-b^\top (S - \bar{\lambda} H)^{-1} b > 0$. To see why this is the case, for any nonzero $v \in \mathbb{R}^2$, we write

$$v^\top (S - \bar{\lambda} H) v = v^\top (S - \lambda^+ H) v - v^\top (\bar{\lambda} - \lambda^+) H v, \tag{22}$$

where the second quadratic form is negative definite because H is positive definite and $\bar{\lambda} > \lambda^+$. We now show that the first quadratic form in (22) is negative semidefinite. Since, by definition, λ^+ is the largest

characteristic value of the regular pencil $S - \lambda H$, we have that (see (Gantmacher 1977))

$$\max \frac{v^\top S v}{v^\top H v} = \lambda^+,$$

from which $v^\top (S - \lambda^+ H) v \leq 0$. Thus, the first quadratic form in (22) is negative semidefinite.

We have thus shown that for $\mathcal{N}$ to be positively invariant one must necessarily have $\bar{\lambda} < 0$ and hence $\lambda^+ = \lambda_{max}(H^{-1}S) < 0$. As seen in the proof of Lemma 2, part (iii), $\lambda^+ < 0$ if and only if $\lambda_{max}(S) < 0$. ■

The lemma above is useful because it is readily seen that S is negative definite if and only if H is the solution to a Lyapunov equation for A. This fact is used in Section 5.2 to find H.

The considerations above lead to an algorithm, summarized in Procedure 2, to determine the range of operation of the platen.

Procedure 2: Dynamic Feedback Linearization

1. Fix an operating region of interest for the vertical dynamics (x_1, x_2) and choose $\hat{U}$ so that $\hat{\mathcal{D}} = \left\{(x_1, x_2, z) : \hat{R}(x_1, x_2, z) \geq 0, L_4(x_1) \neq 0, L_1(x_1) \neq 0\right\}$ contains it
2. Choose $K \in \mathbb{R}^{2\times 4}$ and find the feasible horizontal range of the platen $\Omega^2_{d_2}$ as in items 3 and 4 in Procedure 1
3. Pick positive real numbers k_1, k_2, k_3 such that A is Hurwitz and choose a positive definite matrix H, a 3×1 vector C, and R such that
   (a) $\mathcal{N} = \{(x_1, x_2, z) : [x_1 - C_1 \ x_2 - C_2 \ z - C_3] H [x_1 - C_1 \ x_2 - C_2 \ z - C_3]^\top \leq R\} \subset \hat{\mathcal{D}}$
   (b) Setting $b = \frac{1}{2} H A [0 \ -C_2 \ -C_3]^\top$ in Lemma 2, $\mathcal{N}$ is positively invariant
4. Choose x_1^d such that $(x_1^d, 0, 0) \in \mathcal{N}$ and, using Lemma 2, check whether $\mathcal{N}$ is a feasible vertical operating range
5. Define the dynamic feedback controller

$$\begin{aligned}
\begin{bmatrix} u_1 \\ u_2 \end{bmatrix} &= -\begin{bmatrix} 0 & \frac{1}{2L_1(x_1)} \\ \frac{1}{L_1(x_1)} & 0 \end{bmatrix} K \tilde{\mathbf{x}}^2 \\
u_3 &= 0 \\
u_4 &= -\frac{L_3(x_1) + \sqrt{R(\tilde{\mathbf{x}}, z)}}{2L_4(x_1)} \\
\dot{z} &= -k_1 \tilde{x}_1 - k_2 \tilde{x}_2 - k_3 z
\end{aligned} \tag{23}$$

Lemma 4 *Choose H, C, R, and k_1, k_2, k_3 according to item 3 in procedure 2. Then, for any x_1^d chosen as in item 4 of the procedure, the equilibrium $\mathbf{x} = \mathbf{x}^d$ of the closed-loop system (6), (23) is asymptotically stable and the set $\mathcal{N} \times \Omega^2_{d_2}$ is contained in its domain of attraction.*

Proof: It is sufficient to notice that the choice of H, C, R, and k_1, k_2, k_3 in item 3 of the procedure

μ_0	$4\pi \cdot 10^{-7}$	μ_{rec}	1.1000
p	2	p_m	4
W/p	300	t_1	$19.05 \cdot 10^{-3}$m
b_0	$12.07 \cdot 10^{-3}$m	k_{w1}	1
w_c	$57.15 \cdot 10^{-3}$m	τ	$57.15 \cdot 10^{-3}$m
τ_p	$28.575 \cdot 10^{-3}$m	h_m	$2 \cdot 10^{-3}$m
σ_m	$8.36 \cdot 10^5$	M_p	1.92Kg
L_A	0.05 m	–	–

Table 1: Various parameters used in the simulations.

guarantees, by Lemma 2, that there exists at least one choice of x_1^d (namely, $x_1^d = C_1$) such that $\mathcal{N}$ is positively invariant. ■

Remark 3: Once H, C, R, and k_1, k_2, k_3 have been chosen, it is easy, in practice, to find the interval $\mathcal{I} \subset \mathbb{R}$ such that, $\forall x_1^d \in \mathcal{I}$, $\mathcal{N}$ is positively invariant. This can be done by varying x_1^d in a neighborhood of C_1 and repeatedly checking the conditions in Lemma 2.

5 Simulation Results

This section presents the simulation results for each of the controllers investigated in this paper. For our simulations we utilize the parameters specified in Table 1.

5.1 Lyapunov-Based Control

Following Procedure 1, we first find the set $\mathcal{X}_1$, depicted in Figure 6. Suppose one wants to stabilize the air-gap of the platen at $x_1^d = 0.0115$m, which is a point in $\mathcal{X}_1$. With this choice, we get $U^* = 368.34$, and select $\hat{U} = 87$. In general, the smaller $\hat{U}$, the smaller the horizontal operating range is, and the larger the vertical operating range of the platen is. Next, we select K in (8) to solve the linear quadratic regulator problem for the pair (A_c, B_c), with $Q = R = I_{4\times 4}$ (one could use pole assignment), obtaining

$$K = \begin{bmatrix} 1 & 1.73 & 0 & 0 \\ 0 & 0 & 1 & 1.73 \end{bmatrix}.$$

Following item 3, we get $d_2 = 50.52$. Figure 7 depicts the projection of the horizontal range of operation, $\Omega^2_{d_2}$, onto the $(\tilde{x}_3, \tilde{x}_4)$ plane (its projection onto the $(\tilde{x}_5, \tilde{x}_6)$ plane is identical). The figure shows that the horizontal range of operation around *any given* set point is about ±4m. Given that the typical horizontal range of the device in practice is less than 1/2 meter, we conclude that the nonlinear controller (7) does

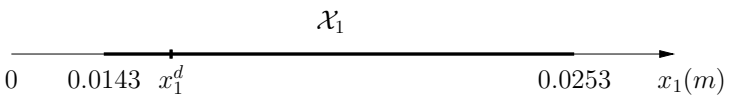

Figure 6: The set $\mathcal{X}_1$ and a choice of $x_1^d \in \mathcal{X}_1$.

not place any restriction on the horizontal operating range. Next, choosing $\tilde{\epsilon} = 2 \cdot 10^5$ and $d_1 = 4.5 \cdot 10^{-6}$

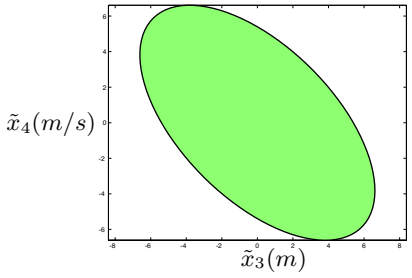

Figure 7: Projection of $\Omega_{d_2}^2$ onto the $(\tilde{x}_3, \tilde{x}_4)$ plane

we obtain the set $\Omega_{d_1}^1 \subset \hat{\mathcal{D}}$ depicted in Figure 8a. The choice of $\tilde{\epsilon}$ satisfies the requirement in item 6 of Procedure 1. Figure 8a also depicts phase curves of the closed-loop vertical dynamics (9) for several initial conditions, showing that the *guaranteed* vertical range of operation around the chosen set point is about ± 0.0025m. Figure 8b displays the sets $\Omega_{d_1}^1$ and $\hat{\mathcal{D}}$, together with few phase curves, when $x_1^d = 0.0225$m. Here $\hat{U}$, d_2, and $\tilde{\epsilon}$ are the same as before, whereas $d_1 = 7 \cdot 10^{-6}$. Figures 8a and 8b show that the size of the sets $\Omega_{d_1}^1$ and $\hat{\mathcal{D}}$ depend on the location of the set point. This is the main drawback of controller (7).

5.2 Dynamic Feedback Linearization

Following Procedure 2 we first need to choose $\hat{U}$. To allow for a comparison with the Lyapunov-based design, we set the same values of $\hat{U}$ and K as in Section 5.1. These yield the same horizontal operating range $\Omega_{d_2}^2$ whose projection onto the $(\tilde{x}_3, \tilde{x}_4)$ plane is depicted in Figure 7. Next, referring to item 3, we need to fit an ellipsoid in $\hat{\mathcal{D}}$ satisfying the invariance properties in item 3b. We plot the set $\hat{\mathcal{D}}$ (see Figure 9a) and choose the center of the ellipsoid to be at $C = [1.70 \cdot 10^{-2} \ 0 \ 0]^\top$. We then need to find scalars k_1, k_2, k_3, a positive definite matrix H and a positive real number R such that, (1), A is Hurwitz, (2), the ellipsoid $\mathcal{N}$ is contained in $\hat{\mathcal{D}}$ and, (3), $\mathcal{N}$ is positively invariant when $x_1^d = C_1$ and, thus, when $b = 1/2HA[0 \ -C_2 \ -C_3]^\top = 0$. When $b = 0$, checking positive invariance of $\mathcal{N}$ amounts to guaranteeing that

$$S = 1/2(HA + A^\top H) \tag{24}$$

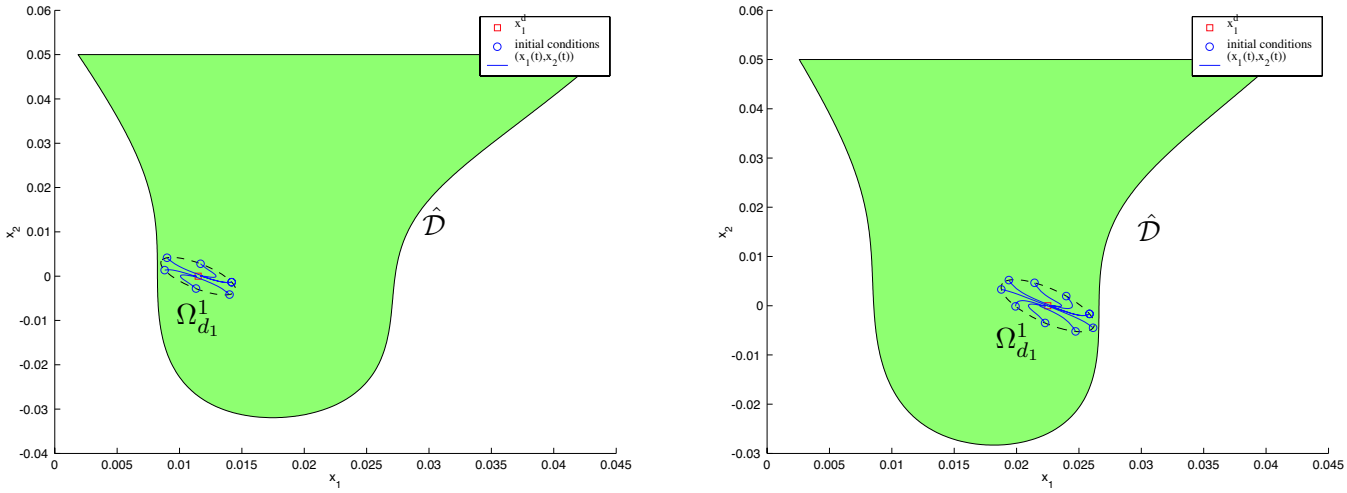

(a) (b)

Figure 8: Lyapunov control: Phase curves of the closed-loop system (9) for two different set points.

is negative semidefinite (see Lemma 2, part (iii)). As remarked earlier, (24) is a Lyapunov equation for A which is guaranteed to have a solution, H, as long as A is Hurwitz. We can find H fulfilling the requirement in item 3b as follows. Choose k_1, k_2, k_3 so that A is Hurwitz, pick a negative definite matrix S and solve the Lyapunov equation (24) to get a positive definite H. Next, choose R so that the associated ellipsoid $\mathcal{N}$ is contained in $\hat{\mathcal{D}}$. Different choices of k_1, k_2, k_3, and S yield different matrices H. By trial and error, one can select H so that $\mathcal{N}$ approximates $\hat{\mathcal{D}}$ to a reasonable degree. We choose $k_1 = 10^3$, $k_2 = 1.11 \cdot 10^3$, $k_3 = 111$ and $S = -diag[10^3, 10^3, 0.8]$. These yield

$$H = \begin{bmatrix} 2.12 \cdot 10^3 & 127.4 & 1 \\ 127.4 & 129.9 & 1 \\ 1 & 1 & 0.0164 \end{bmatrix}.$$

Finally, choosing $R = 0.12$ we obtain $\mathcal{N} \subset \hat{\mathcal{D}}$ shown in Figure 9. The choice of parameters above guarantees that, when $x_1^d = C_1 = 1.70 \cdot 10^{-2}$m, $\mathcal{N}$ is positively invariant. As pointed out in Remark 3, by varying x_1^d in a neighborhood of C_1 and repeatedly checking the conditions in Lemma 2, one finds an interval $I \subset \mathbb{R}$ such that $\forall x_1^d \in \mathcal{I}$, $\mathcal{N}$ is positively invariant. By so doing we find that

$$I = [0.0115\text{m}, 0.0225\text{m}]. \tag{25}$$

In conclusion, for *any* $x_1^d \in I$, the set $\mathcal{N}$ is the vertical operating range of the platen. Figure 9 displays few phase curves of the closed-loop vertical dynamics when $x_1^d = 0.0120$m, together with the set I.

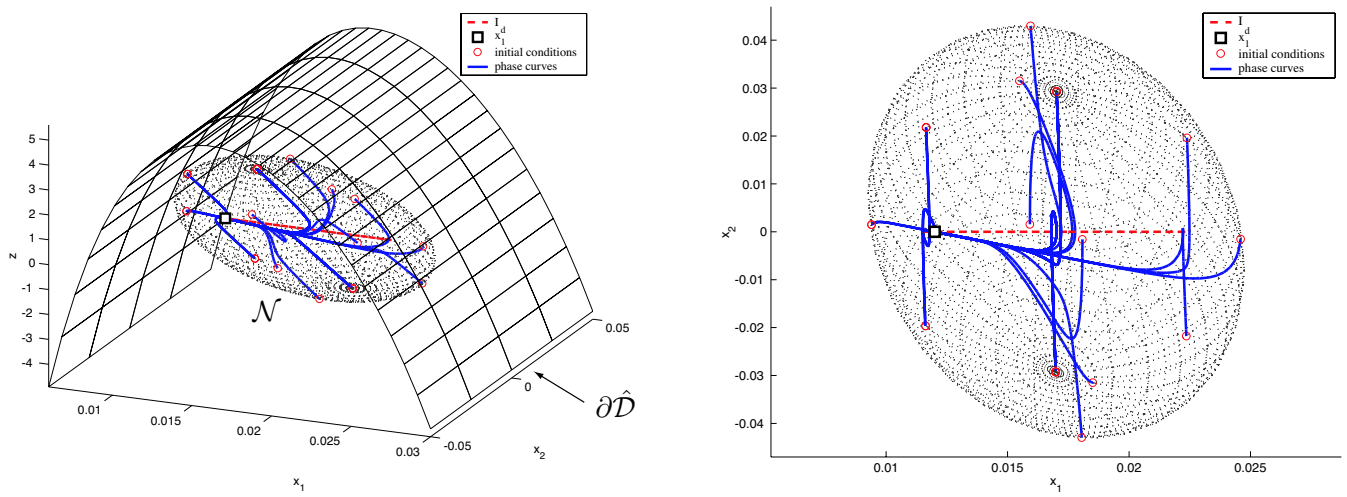

Figure 9: Dynamic feedback linearization: Two different views of some phase curves of the closed-loop system (14).

Finally, we compare the dynamic feedback linearizing controller in (23) with a linear controller,

$$u = \mathcal{K}(\mathbf{x} - \mathbf{x}^d),$$

obtained by linearization and LQR design. The main drawback of linearization-based controllers is that the size of the domain of attraction varies with the set-point around which linearization is performed. Furthermore, it may not be possible to use a single linear controller to stabilize all set-points in the range of interest. This is an undesirable feature in motion control applications whenever a large range of operation is sought. To illustrate this, we design an LQR controller around the set point $\mathbf{x}^d = [0.0115\ 0\ 0\ 0\ 0\ 0]^\top$. We pick

$$Q = diag[5 \cdot 10^3\ 5 \cdot 10^3\ 3\ .1\ 3\ .1],\ R = I_{4\times 4},$$

to make sure that the performance with the resulting LQR controller near the set point is comparable to that achieved using (23). Next, we use the *same* linear controller to stabilize the set-point $\mathbf{x}^d = [0.0225\ 0\ 0\ 0\ 0\ 0]^\top$. We know from the previous discussion that the dynamic feedback linearizing controller (23) can be used to stabilize *both* set-points above and guarantees in both cases that $\mathcal{N}$ is positively invariant. This is confirmed by the simulation results depicted in Figure 10a. The same initial conditions are then used to test the LQR controller. Figure 10b shows that the performance of the LQR controller in stabilizing the first set-point is comparable to that of the nonlinear controller. On the other hand, when using the same controller to stabilize the second set-point, Figure 10b shows that some of the phase curves leaving from $\mathcal{N}$ are unbounded. This problem could be overcome by using gain scheduling, but then the issue of rigorously determining the range of operation would arise.

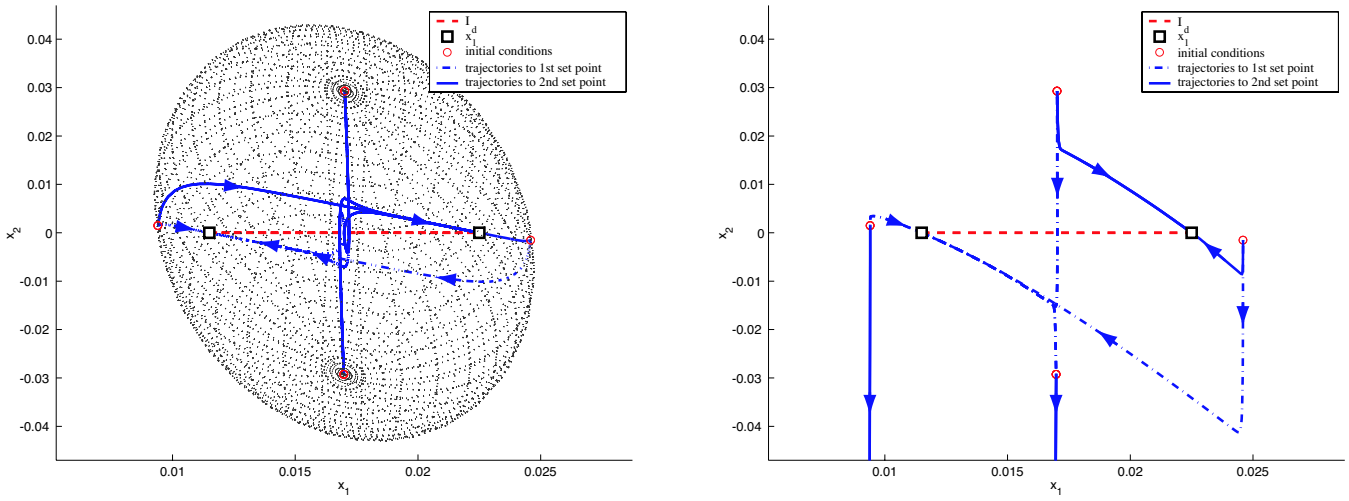

(a) (b)

Figure 10: Phase curves of the closed-loop system with (a) nonlinear and (b) linear feedback approaching two different setpoints.

6 Conclusions

We have presented two nonlinear control strategies to regulate the position of the platen to a desired set point. In both cases we have outlined a procedure to estimate the domain of attraction of the set point which provides the guaranteed range of operation of the device. Our simulation results in Section 5 show that both controllers do not restrict the horizontal range of operation.

On the other hand, air-gap control presents a greater challenge, making the estimation of the vertical operating range crucial. The vertical operating range of the Lyapunov controller in Section 4.1 depends on the choice of x_1^d and gets smaller as $(x_1^d, 0)$ gets closer to the boundary of the set $\hat{\mathcal{D}}$ (see Figure 8). This is an undesirable feature of the controller in Section 4.1. The dynamic feedback linearizing controller in Section 4.2 overcomes this problem because it allows one to find (through Procedure 2) an operating range $\mathcal{N}$ which is valid *for all* choices of x_1^d in an interval I which can be computed *a priori* (in our simulations $I = [0.0115\text{m}, 0.0225\text{m}]$). A comparison between Figures 8 and 9b shows that the operating range of the dynamic feedback linearizing controller is larger than that of the Lyapunov controller for both choices of the set point in Figures 8a and 8b.

7 Aknowledgements

We are grateful to R. B. Owen for his useful comments and suggestions.

References

Gantmacher, F. R.: 1977, *The Theory of Matrices*, Chelsea Publishing Company, New York.

Gieras, J. F. and Piech, Z. J.: 2000, *Linear Synchronous Motors: transportation and automation systems*, CRC Press, Boca Raton, FL, USA.

Kim, W. and Trumper, D.: 1998, High-precision levitation stage for photolithography, *Precision Engineering* **22**, 66–67.

Nasar, S. and Xiong, G.: 1988, Determination of the field of a permanent-magnet disk machine using the concept of magnetic charge, *IEEE Transactions on Magnetics* **24**(3), 2038–2044.

Nasar, S. and Xiong, G.: 1989, Analysis of fields and forces in a permanent magnet linear synchronous machine based on the concept of magnetic charge, *IEEE Transactions on Magnetics* **25**(3), 2713–2719.

Shan, X., Kuo, S.-K., Zhang, J. and Menq, C.-H.: 2002, Ultra precision motion control of a multiple degrees of freedom magnetic suspension stage, *IEEE/ASME Transactions on Mechatronics* **7**(1), 67–78.

Tsai, K.-Y. and Yen, J.-Y.: 1999, Servo system design of a high-resolution piezo-driven fine stage for step-and-repeat microlithography systems, *The 25th Annual Conference of the IEEE Industrial Electonics Society*, Vol. 1, pp. 11–16.

Zhu, Z. and Howe, D.: 1993, Instantaneous magnetic field distribution in brushless permanent magnet DC motors, part III: Effect of stator slotting, *IEEE Transactions on Magnetics* **29**(1), 143–151.